HHS Public Access

Author manuscript

Bone. Author manuscript; available in PMC 2017 March 01.

Published in final edited form as:

Bone. 2016 March ; 84: 245–252. doi:10.1016/j.bone.2015.12.051.

Prevention of radiation-induced bone pathology through combined pharmacologic cytoprotection and angiogenic stimulation

Alexis Donneys, MD, MS[1], **Noah S. Nelson, BS**[1], **Joseph E. Perosky, MS**[1], **Yekaterina Polyatskaya, MD**[1], **Jose J. Rodriguez, MD**[1], **Christian Figueredo, BS**[1], **Cheyenne A. Vasseli, BS**[1], **Hannah C. Ratliff, BS**[1], **Sagar S. Deshpande, BS**[1], **Kenneth M. Kozloff, PhD**[1], and **Steven R. Buchman, MD**[1]

[1]University of Michigan, Ann Arbor, Michigan, USA

1. Introduction

Adjuvant radiotherapy is an effective treatment modality that is utilized by approximately half of the cancer patient population (1). Despite its benefits, radiotherapy is known to have caustic effects on healthy tissues through mechanisms that disrupt normal tissue vascularity and cellularity (2,3). Bone is particularly susceptible to these detrimental effects because of a baseline metabolic turnover rate that is comparatively slower than that of other tissue types (4). This slow metabolism can help to mask clinical symptoms until pathologies progress beyond the point of prevention or early intervention. These aberrant effects can lead to debilitating pathologies such as osteoradionecrosis, pathologic fractures and associated non-unions (5).

Although the underlying mechanisms of radiation injury have been studied extensively, currently, no clinically accepted medical therapies exist to prevent the deleterious effects of radiation on normal osseous tissues (6). Pharmacologic strategies designed to manipulate and optimize the cellular and vascular environments within irradiated bone are therefore warranted.

Previously, our laboratory has utilized amifostine–a radioprotectant–and deferoxamine–an angiogenic stimulant as targeted interventions to selectively preserve osteocyte viability and augment vascularity, respectively, in an animal model of mandibular fracture repair following radiation exposure. Our results demonstrated the ability of these singular therapies to partially temper the effects of radiation on mechanisms of fracture healing as measured with 3D angiographic modeling, histology, radiomorphometrics and mechanical testing (7–10).

Corresponding Author: Alexis Donneys, MD, MS, Craniofacial Research Laboratory, 109 Zina Pitcher Place, Room 2268 BSRB, Ann Arbor, MI 48104, Phone: 215-219-8748, alexisd@med.umich.edu.

Disclosures: All authors state that they have no conflicts of interest.

Although our results with singular therapies are promising, complete restoration of our outcome measures and clinical assessments to that of normal, non-irradiated bone has yet to be achieved. The purpose of this study was to improve upon the success of singular therapies in an effort to reach more consistently normalized outcome measures by combining these targeted therapeutic interventions. We hypothesized that the cellular radio-protective nature of amifostine, in combination with the angiogenic stimulation of deferoxamine would act in a complementary manner to improve upon irradiated fracture metrics and normalize outcome measures to reach non-irradiated fracture levels. Here we report 3D angiographic modeling, histology, Bone Mineral Density Distribution (BMDD) and biomechanical metrics of bone healing.

2. Materials and Methods

2.1 Study design

All animal experimentation was approved by the University of Michigan's Committee for the Utilization and Care of Animals (UCUCA), and conducted in accordance with the guidelines published in the Guide for the Care and Use of Laboratory Animals: Eighth Edition. In order to facilitate the incorporation of destructive outcome measures, two cohorts of animals undergoing identical experimentation (with the exception of outcomes testing) represent each group. Animals in cohort 1 underwent 3D angiographic modeling and histology, while animals in cohort 2 underwent μCT imaging for BMDD analysis and mechanical testing.

Twelve-week-old male Sprague Dawley rats (n=117) were divided into 5 groups: fracture (Fx), irradiated fracture (XFx), irradiated fracture treated with deferoxamine alone (DFO), irradiated fracture treated with amifostine alone (AMF), and irradiated fracture treated with amifostine plus deferoxamine combination therapy (Combined). In Cohort 1 (n=60), animals were equally divided between groups (n=12/group). Cohort 2 (n=57) consisted of: Fx (n=5), XFx (n=14), DFO (n=15), AMF (n=10) and Combined (n=13). All irradiated groups received a previously established human equivalent dose of radiotherapy (HEDR) two weeks prior to surgery. AMF and Combined groups received an injection of subcutaneous amifostine immediately prior to each radiation therapy session. Following a two-week recovery period, all groups received an osteotomy posterior to the 3rd molar of the left hemi-mandible, along with the placement of an external fixator device. The DFO and Combined groups then received injections of deferoxamine directly into the fracture callus every other day from post-operative day 4–12 for a total of 5 doses. Following a 40-day healing period, animals were sacrificed, and mandibles were dissected for outcomes testing. (see Figure 1).

2.2 Amifostine injection

A subcutaneous amifostine injection (100 mg/kg) was given forty minutes prior to radiation therapy once daily for five consecutive days according to the radiation therapy schedule outlined below. The dosage was derived from an extensive review of the literature and previous work in our laboratory. We further optimized these doses and dosing schedules for use in this animal model (11, 12).

2.3 Radiation procedure

Induction of anesthesia was achieved with an oxygen/isoflurane mixture. Left hemi-mandibles were irradiated using a Philips RT250 orthovoltage unit (250 kV X-rays, 15 mA; Kimtron Medical, Woodbury, CT). Our selected region of interest (ROI) spanned a 2 mm distance posterior to the third molar, which corresponded to the future site of osteotomy. Lead shielding ensured localized delivery and protection of surrounding tissues. A previously described HEDR, developed with the guidance of the Department of Radiation Oncology at the University of Michigan, was utilized (13). A fractionated dose of 7 Gy per day was administered over 5 days for a total of 35 Gy, which is comparable to 70 Gy in human mandibular high-dose radiotherapy. Animals were allowed a 14-day recovery period after radiation exposure prior to osteotomy surgery.

2.4 Surgical procedure

Animals were prepared for surgery and underwent external placement of a custom mandibular fixator device followed by osteotomy directly behind the third molar on the left hemi-mandible as previously described (14, 15). Four hours after osteotomy, the fixator device was set to a 2 mm fixed distance for the remainder of the experiment.

2.5 Deferoxamine injection

Two hundred μM deferoxamine in 300 μL of normal saline was injected directly into the fracture site every other day starting on post-operative day 4 and continuing through postoperative day 12. This dosage was selected from a review of the literature concerning the use of deferoxamine in long bone animal models and modified according to our experimental use in the rat mandible (16–20). The time frame for administration was chosen to correlate with the reasonable time period for the initiation of angiogenesis in a murine fracture model (21–23).

2.6 3D angiographic modeling

Only rats in cohort 1 were anesthetized prior to thoracotomy and underwent left ventricular catheterization. Perfusion with heparinized normal saline followed by pressure fixation with normal buffered formalin solution ensued and ensured euthanasia. After fixation, the vasculature was injected with Microfil (MV-122, Flow Tech, Carver, Mass.), and mandibles were subsequently harvested en bloc and demineralized using Cal-Ex II solution (Fisher Scientifics; Fairlawn, NJ). Leeching of mineral was confirmed with serial radiographs to ensure adequate demineralization prior to scanning. μCT images were obtained using 80kVp, 80mA and 1100 ms exposures. Three hundred and ninety-two projections were taken at a resolution of 18-micron voxel size. Utilizing GE's Microview 2.2 software, scans were reconstructed and reoriented in a 3D x, y and z plane. The ROI was then cropped and splined for analysis. Due to demineralization, only the vessels perfused with Microfil appeared on the μCT scan. Vessel Volume (VVF) and Vessel Number (VN) were assessed (24).

2.7 Histological analysis

All specimens underwent 70% ethanol fixation at 4°C and were decalcified with Cal-Ex II solution. The specimens were then vacuum processed, filtrated, and embedded in Paraplast Plus (i.e., paraffin containing dimethylsulfoxide; McCormic Scientific, Richmond, Ill.) as previously described (39). Embedding molds (22 × 40 mm) were used and stored overnight at 4°C. Blocks were sectioned coronally from anterior to posterior spanning the ROI (a 2 mm distance posterior to the third molar, which corresponded to the site of osteotomy). Seven μm thick sections were taken through the ROI on a Leica Reichert-Jung microtome (model 2030; Biocut, Bensheim, Germany), and mounted on glass slides (Fisherbrand Superfrost Plus; Fisher Scientific). Sections were surface-stained with Gomori's one-step trichrome. Osteocyte count (OC) was performed with a light microscope interfaced with a digital camera connected to a computer. Our ROI was superimposed onto the digital image using Bioquant NOVA Osteo version 7 (R&M Biometrics, Nashville, Tenn.). Nine high-power field images were randomly selected per ROI using 16x magnification. The high-power field images measured 295 × 366 pixels and were stored as TIFF files. Three independent reviewers performed the point counting of osteocytes.

2.8 Bone mineral density distribution analysis (BMDD)

μCT images of the dissected mandibles were obtained using 80kVp, 80mA and 1100 ms exposures (μCT, eXplore Locus SP, GE Healthcare Pre-Clinical Imaging, London, ON, Canada). Three hundred ninety-two projections were taken at a 45-micron voxel size for bone analysis. Utilizing the μCT images and GE's Microview 2.2 software, BMDD histogram data was generated for the ROI using a predefined threshold of 800–4000 Hounsfield Units (HU). This threshold identifies voxels as being bone within this volume and is typically used in our models for the normal distribution of bone density as previously described (25). An average histogram was generated for each group, and metrics were derived in accordance with previously established parameters (25–28).

2.9 Mechanical testing

After imaging, mandibles were potted and loaded to failure in uniaxial monotonic tension at 0.5 mm/s using a servohydraulic testing machine (858 Minibiox II; MTS Systems Corporation, Eden Prairie, MN, USA). Crosshead displacement was recorded by using an external variable differential transducer (LVDT; Lucas Schavitts, Hampton, VA, USA), and load data were collected with a 100-lb load cell (Sensotec, Columbus, OH, USA). Data were sampled at 200 Hz on a TestStar system (TestStar IIs System version 2.4; MTS Systems Corporation). Load-displacement curves were analyzed for whole bone yield (Y), stiffness (S), ultimate load (UL) and failure load (FL) using custom computational code (MATLAB 7.11; Mathworks Inc., Natick, MA, USA).

2.10 Statistical analysis

All data were presented as group means ± 1 SD. One-way ANOVA was used to compare means for all reported metrics. Significance was defined as $p < 0.05$. Levene's test was used to exclude inequality of SD's. Post hoc analysis for multiple group comparisons included

Tukey's test or Games-Howell analysis if Levene's test indicated inequality of variance. All statistical analysis was conducted using SPSS 20 software (IBM).

3. Results

3.1 Vascularity data

There was a significant reduction in VVF and VN for the XFx group as compared to the Fx group indicating a decreased vascularity with radiation exposure ($p = 0.042$ and 0.015, respectively). All therapies improved upon XFx levels (VVF: $p = 0.045$, 0.04 and 0.024; VN: $p = 0.025$, 0.020 and 0.041 for DFO, AMF and Combined, respectively), there were no differences observed between any of the therapies (VVF: $p = 0.802$, 0.971 and 0.479; VN: $p = 0.874$, 0.984 and 0.983 for DFO vs. AMF, Combined vs. AMF and Combined vs. DFO, respectively), and all therapies reached the levels of the non-irradiated fracture group (Fx) (VVF: $p = 0.897$, 1.0 and 0.949; VN: $p = 1.0$, 0.883 and 0.998 for DFO, AMF and Combined, respectively), implying that both AMF and DFO are equally effective in maintaining vascularity at the fracture site despite differing mechanisms of action, and that these effects are maintained in the combination therapy (see Figure 2).

3.2 Histology data

A significant reduction in OC was observed for the XFx group as compared to the Fx group, indicating decreased bone cellularity with radiation exposure ($p = 0.001$). All therapies improved upon XFx levels (OC: $p = 0.001$ for all three therapies). However, a significant difference between the Combined group and DFO was observed, as well as a trending difference between AMF and DFO, where both the AMF and Combined OC's were higher than DFO (OC: $p = 0.001$ and 0.078 for Combined and AMF vs. DFO, respectively). This may imply that the ability to preserve osteocytes is an effect that is more pronounced with AMF therapy than with DFO alone, and that this effect is maintained in the combination therapy (see Figure 3).

3.3 BMDD data

Bone Mineral Density Distribution histograms were used to visualize and delineate where the changes in mineralization patterns existed between the groups. We found that the histogram curve of the Combined group more closely matched the curve of Fx than any of the other treatment groups. We also observed significant differences in the 5^{th} percentile of mineralization (*m*Low) and the mineralization slope of decline (*m*SOD). *m*Low represents early, immature mineral within the bone whereas *m*SOD is an indicator of the higher radiodensities within bone, which represent more mature mineral. For both parameters, there was a significant reduction observed for the XFx group as compared to the Fx group (*m*Low: $p = 0.006$ and *m*SOD: $p = 0.005$). All therapies improved upon XFx levels for *m*Low ($p = 0.047$, 0.018 and 0.002 for DFO, AMF and Combined, respectively). However, AMF failed to do so for the *m*SOD metric ($p = 0.630$). Further, significant differences were observed between AMF and Combined for *m*Low ($p = 0.037$), and between AMF and both DFO and Combined groups for *m*SOD ($p = 0.027$ and 0.018 for DFO and Combined, respectively). These findings highlight the effect of DFO in specifically preserving immature and mature mineral patterns within irradiated bone (see Figure 4).

3.4 Mechanical testing data

In accordance with our other metrics, reductions across mechanical parameters were observed as a result of radiation administration. Specifically, there was a significant reduction in Y, S, UL and FL when comparing Fx to XFx ($p = 0.049$, 0.022, 0.036 and 0.024, respectively). While DFO and Combined groups improved upon XFx levels for these metrics, AMF did not (Y: $p = 0.001$, 0.0081, 0.030; S: $p = 0.003$, 0.055, 0.004; UL: $p = 0.003$, 0.097, 0.033 and FL: $p = 0.003$, 0.084, 0.026 for DFO, AMF and Combined, respectively). Further, a significant difference was observed between AMF and Combined for S ($p = 0.047$). Collectively, this may imply that the maintenance of structural integrity and mechanical strength are effects that are more pronounced with DFO therapy than with AMF alone, and that these effects are maintained in the combination therapy (see Figure 5).

4. Discussion

To date, there are no existing pharmacologic options for the prevention of radiation-induced bone pathologies. Current and past treatment paradigms have been largely unsuccessful in dealing with these complex diseases. Hyperbaric oxygen therapy (HBO), once considered the standard therapeutic modality by authors such as Marx, has not been proven to be an efficacious preventative strategy in these regards (29). Since there are no preventative measures, patients typically present at a point in time beyond the possibility of early intervention and non-invasive treatment. Consequently, therapeutic intervention typically occurs after irreversible damage has already taken place (30, 31). The current standard of care for advanced osteoradionecrosis, pathologic fractures and non-unions in the setting of radiotherapy is surgical debridement of necrotic bone, followed by autologous free tissue transfers. However, these operations are highly invasive, costly, complex and associated with high post-operative rates of morbidity (32–36).

In this study, we utilized a novel drug combination of amifostine, a cellular radioprotectant, and deferoxamine, an angiogenic stimulant, to simultaneously target the cellular and vascular niches within irradiated bone in a rat model of mandibular fracture repair following radiation exposure. We chose our therapies based on their demonstrated ability to impact these mechanisms and potentially affect a restoration of bone healing. In particular, because vascularity is such an integral part of maintaining viable cells, we felt that not only protecting the existing cells with amifostine, but restoring an adequate blood supply to the site of fracture healing with deferoxamine may afford a method for promoting osteocyte survival and optimized healing despite the effects of radiotherapy. Furthermore, recent cellular and molecular studies have shed considerable light on the effects of radiation on angiogenic mechanisms. While it is commonly known that radiation is detrimental to existing vascularity within irradiated bone, there is emerging evidence that radiation also affects endothelial cell function, and their angiogenic capacity. Imaizumi, et al. provide *in vivo* evidence that radiation prevents VEGF and FGF-2 induced angiogenesis, and *in vitro* evidence showing suppressed endothelial cell proliferation, migration and sprouting (37). Our previous results utilizing live cell imaging of irradiated endothelial cells in Matrigel corroborate these observations. We observed impaired migration, sprouting and lack of organization *in vitro*. These effects were subsequently remediated with the addition of

deferoxamine, prompting us to examine its utility in the animal model reported here (10, 38).

The US Army developed amifostine during the Cold War as a preventative measure in case of nuclear war. It remains the most extensively studied and clinically utilized radioprotectant since that time period (39). Its clinical utility with regards to radiation toxicity is predominantly for the prevention of xerostomia, a common side effect of radiotherapy in HNC patients (40). Amifostine is an organic triphosphate prodrug that becomes active upon dephosphorylation in normal tissues. Once active, amifostine's metabolite, WR-1065, scavenges radiation-induced reactive oxygen species that are responsible for much of the damage to healthy tissue cellularity and vascularity. Research has demonstrated that amifostine selectively protects non-malignant tissues due to a higher alkaline phosphatase activity, pH, and vascular permeation of normal tissues in comparison to malignant tissues (41). To our knowledge, the earliest research regarding its use for the protection of irradiated osseous tissues was conducted by Capizzi et al. who demonstrated its cytoprotective effects on bone marrow stem cells (42). Subsequently, Forrest et al. demonstrated its ability to prevent radiation-induced craniofacial growth restriction *in vivo*, and Damron et al. demonstrated its use for the prevention of radiation induced growth plate restriction (43–45).

Deferoxamine is an iron chelator clinically utilized for the treatment of transfusion-related iron-overload (46). Investigators have also discovered that the drug exhibits angiogenic properties through an induction of the HIF-1α pathway and subsequent up-regulation of VEGF and other downstream mediators of angiogenesis (47, 48). Regarding its use in bone, there is evidence supporting the ability of deferoxamine to enhance osseous healing through demonstrated augmentation of vascularity, bone quality, and mechanical strength in various murine long-bone fracture and distraction models (16–18). These findings prompted us to investigate the potential of deferoxamine to remediate radiation injury in our model.

Utilizing this combined pharmacologic strategy, our specific goals were: 1- To improve upon XFx metrics; 2- To normalize metrics to reach Fx (non-treated/non-radiated fracture) levels; and 3- To improve upon the effects of each singular therapy. Our quantitative metrics indicate that only the Combined group consistently achieved all three benchmarks. Across the board, the Combined group improved upon XFx levels, normalized all reported metrics and was consistently as good as, or superior to the other treatment groups. As a note, however, the Combined therapy was never better than both singular therapies, reasonably indicating that the observed effects were a result of the therapeutic contributions of amifostine and deferoxamine, as opposed to novel effects elicited by the combination.

Although DFO also consistently improved upon XFx levels and normalized the reported metrics, it was inferior to the combined therapy for osteocyte count. Lastly, although AMF improved upon radiation levels for metrics of vascularity and histology, it failed to improve upon radiation levels for the BMDD 5^{th} percentile of mineralization (*m*Low), and all reported mechanical metrics.

Through our data, we were also able to elucidate the strengths and weaknesses of each therapeutic contribution. Interestingly, both amifostine and deferoxamine maintained

vascularity despite their differing mechanisms of action (i.e. cytoprotection vs. angiogenic stimulation, respectively). While the angiogenic capacity of deferoxamine has been demonstrated, it is reasonable to deduce that amifostine also plays a role in the preservation of endothelial cells and their subsequent angiogenic mechanisms, although focused *in vitro* studies will be needed to substantiate these findings and offer further insights. Deferoxamine was less effective than amifostine at preserving osteocytes. However, BMDD and mechanical data demonstrated that deferoxamine was superior to amifostine in preserving early and late mineralization patterns and mechanical strength at the irradiated fracture site. Upon further consideration, our BMDD data visually highlighted the similarities between the mineralization patterns of the Combined group and the Fx group, and demonstrated how the combination therapy functioned to establish a mineralization curve that was very near that of normally healing, non-irradiated bone. Taken together, our observations indicate that both singular therapies exhibited unique strengths that enhanced the combination therapy in a complementary fashion. It is plausible that while amifostine works to preserve the working capacity of existing irradiated cells, deferoxamine works to reestablish the requisite functional vascular channels needed to deliver vital substrates to the site of fracture healing.

We wish to address and clarify limitations to our study. In our design, we utilize an osteotomy in lieu of a naturally occurring fracture. Clinically, pathologic fractures often take years to develop after radiotherapy. Despite the constraints of practicality and time, we have demonstrated that our model effectively recreates the signs of pathologic fracture in a timely and reproducible manner, making it a viable and pertinent platform for pathologic fracture research. Lastly, and most clinically relevant, although the tumorigenic safety of amifostine, particularly regarding its use in the head and neck cancer population, is widely accepted, the angiogenic safety of deferoxamine use in cancer patients has not been well established. In fact, we are not advocating the use of deferoxamine around the time of oncologic management. Instead, its use would be more judicious at a later time, away from the time of tumor resection and radiation, but prior to the typical time-period for the development of radiation-related osseous complications. Despite this, there are several promising studies demonstrating that deferoxamine has anti-tumorigenic properties by depleting rapidly dividing cancerous cells of iron, which is vitally important in DNA replication (49–52). Nonetheless, future studies should be aimed at identifying the tumorigenic safety of deferoxamine and the relevant time period of use for these intended purposes.

In conclusion, radiation-induced bone pathologies are known to cause substantial morbidity, and effective preventative measures are currently lacking. Here we demonstrate a therapeutic strategy for targeting the cellular and vascular niches within irradiated bone with radioprotective amifostine and angiogenic deferoxamine and report the benefits and limitations of each therapy.

Acknowledgments

Funding Information:

This work was supported by grants from the National Institutes of Health R01 (CA12587-01, CA12587-06) to S.R.B., 3R01 CA 125187-07S2 NCI Supplement to Promote Diversity in Health Related Research for A. D., T32-GM008616 to Cynthia L. Marcelo for A.D. and The Plastic Surgery Foundation Pilot Grant to A.D. for proposal titled “Therapeutic Prevention of Radiation Induced Non-Unions.”

The authors thank Mary Davis and Dave Karnak for assistance with the delivery of radiotherapy and Charles Roehm for custom fixator device fabrication.

References and Notes

1. Bernier J, Hall EJ, Giaccia A. Radiation oncology: a century of achievements. Nat Rev Cancer. 2004; 4:737–747. [PubMed: 15343280]
2. Lyons A, Osher J, Warner E, Kumar R, Brennan PA. Osteoradionecrosis A review of current concepts in defining the extent of the disease and a new classification proposal. British Journal of Oral and Maxillofacial Surgery. 2014; 52(5):392–395. [PubMed: 24725905]
3. Baker DG, Krochak RJ. The response of the microvascular system to radiation: a review. Cancer investigation. 1989; 7(3):287–294. [PubMed: 2477120]
4. Marx, Robert E. Osteoradionecrosis: a new concept of its pathophysiology. Journal of Oral and Maxillofacial Surgery. 1983; 41(5):283–288. [PubMed: 6572704]
5. Marx RE, Johnson RP. Studies in the radiobiology of osteoradionecrosis and their clinical significance. Oral Surgery, Oral Medicine, Oral Pathology. 1987; 64(4):379–390.
6. Cao X, Wu X, Frassica D, et al. Irradiation induces bone injury by damaging bone marrow microenvironment for stem cells. Proceedings of the National Academy of Sciences. 2011:201015350.
7. Tchanque-Fossuo CN, Donneys A, Sarhaddi D, et al. The effect of Amifostine prophylaxis on bone densitometry, biomechanical strength and union in mandibular pathologic fracture repair. Bone. 2013; 57(1):56–61. [PubMed: 23860272]
8. Donneys A, Tchanque-Fossuo CN, Blough JT, et al. Amifostine Preserves Osteocyte Number and Osteoid Formation in Fracture Healing Following Radiotherapy. Journal of Oral and Maxillofacial Surgery. Sep.2013 Article in Press. 10.1016/j.joms.2013.09.006
9. Donneys A, Ahsan S, Perosky JE, et al. Deferoxamine Restores Callus Size, Mineralization, and Mechanical Strength in Fracture Healing after Radiotherapy. Plast Reconstr Surg. 2013; 131(5): 711e–719e.
10. Weiss DM, Donneys A, Tchanque-Fossuo CN, et al. Deferoxamine Augments Vascularity and Prevents Osteocyte Depletion Following Radiotherapy in a Mandibular Pathologic Fracture Model. Plast Reconstr Surg. 2012; 130(5S-1):15–16.
11. Tchanque-Fossuo CN, Donneys A, Deshpande SS, et al. Amifostine Remediates the Degenerative Effects of Radiation on the Mineralization Capacity of the Murine Mandible. Plast Reconstr Surg. 2012; 129(4):646e–655e.
12. Tchanque-Fossuo CN, Donneys A, Razdolsky ER, et al. Quantitative Histologic Evidence of Amifostine-Induced Cytoprotection in an Irradiated Murine Model of Mandibular Distraction Osteogenesis. Plast Reconstr Surg. 2012; 130(6):1199–1207. [PubMed: 22878481]
13. Monson LA, Jing XL, Donneys A, et al. Dose-Response Effect of Human Equivalent Radiation in the Mandible. J Craniofac Surg. 2013; 24(5):1593–1598. [PubMed: 24036733]
14. Buchman SR, Ignelzi MA Jr, Radu C, et al. A unique rodent model of distraction osteogenesis of the mandible. Ann Plast Surg. 2002; 49:511–519. [PubMed: 12439020]
15. Tong L, Buchman SR, Ignelzi MA Jr, et al. Focal adhesion kinase expression during mandibular distraction osteogenesis: evidence for mechanotransduction. Plast Reconstr Surg. Jan; 2003 111(1):211–22. discussion 223–4. [PubMed: 12496582]
16. Shen X, Wan C, Ramaswamy G, et al. Prolyl hydroxylase inhibitors increase neoangiogenesis and callus formation following femur fracture in mice. J Orthop Res. 2009; 27:1298–1305. [PubMed: 19338032]
17. Wan C, Gilbert SR, Cao X, et al. Activation of the hypoxia-inducible factor-1alpha pathway accelerates bone regeneration. Proc Natl Acad Sci USA. 2008; 105:686–691. [PubMed: 18184809]
18. Street J, Bao M, deGuzman L, et al. Vascular endothelial growth factor stimulates bone repair by promoting angiogenesis and bone turnover. Proc Natl Acad Sci USA. 2002; 99:9656–9661. [PubMed: 12118119]

19. Farberg AS, Jing XL, Monson LA, et al. Deferoxamine reverses radiation induced hypovascularity during bone regeneration and repair in the murine mandible. Bone. 2012; 50(5):1184–7. [PubMed: 22314387]
20. Donneys A, Farberg AS, Tchanque-Fossuo CN, et al. Deferoxamine enhances the vascular response of bone regeneration in mandibular distraction osteogenesis. Plast Reconstr Surg. 2012; 129(4):850–856. [PubMed: 22456357]
21. AI-Aql ZS, Alagl S, Graves DT, et al. Molecular mechanisms controlling bone formation during fracture healing and distraction osteogenesis. J Dent Res. 2008; 87(2):107–118. [PubMed: 18218835]
22. Glowacki J. Angiogenesis in fracture repair. Clin Orthop Relat Res. 1998; 355(Suppl):S82–S89. [PubMed: 9917629]
23. Aronson J. Temporal and spatial increases in blood flow during distraction osteogenesis. Clin Orthop Relat Res. 1994; (301):124–31. [PubMed: 8156663]
24. Jing XL, Farberg AS, Monson LA, Buchman SR. Radiomorphometric quantitative analysis of vasculature in rat mandible utilizing microcomputed tomography. Plastic and Reconstructive Surgery. 2009; 124(4S):26–27.
25. Donneys A, Nelson NS, Deshpande SS, et al. Quantifying mineralization utilizing bone mineral density distribution in the mandible. The Journal of craniofacial surgery. 2012; 23(5):1502. [PubMed: 22976646]
26. Roschger P. Constant mineralization density distribution in cancellous human bone. Bone. 2003; 32(3):316–3238. [PubMed: 12667560]
27. Hofstaetter JG, Roschger P, Klaushofer K, Kim HKW. Increased matrix mineralization in the immature femoral head following ischemic osteonecrosis. Bone. 2010; 46(2):379–85. [PubMed: 19833243]
28. Roschger P, Lombardi A, Misof BM, et al. Mineralization density distribution of postmenopausal osteoporotic bone is restored to normal after long-term alendronate treatment: qBEI and sSAXS data from the fracture intervention trial long-term extension (FLEX). Journal of bone and mineral research: the official journal of the American Society for Bone and Mineral Research. 2010; 25(1): 48–55.
29. Annane D, Depondt J, Aubert P, et al. Hyperbaric oxygen therapy for radionecrosis of the jaw: a randomized, placebo-controlled, double- blind trial from the ORN96 study group. J Clin Oncol. 2004; 22:4893–900. [PubMed: 15520052]
30. Vissink A, Burlage FR, Spijkervet FKL, Jansma J, Coppes RP. Prevention and treatment of the consequences of head and neck radiotherapy. Critical Reviews in Oral Biology & Medicine. 2003; 14(3):213–225. [PubMed: 12799324]
31. Basu T, Laskar SG, Gupta T, Budrukkar A, Murthy V, Agarwal JP. Toxicity with radiotherapy for oral cancers and its management: A practical approach. Journal of cancer research and therapeutics. 2012; 8(6):72.
32. Coletti D, Ord RA. Treatment rationale for pathological fractures of the mandible: a series of 44 fractures. Int J Oral Maxillofac Surg. 2008; 37(3):215–222. [PubMed: 18023145]
33. McCrory AL, Magnuson JS. Free tissue transfer versus pedicled flap in head and neck reconstruction. Laryngoscope. 2002; 112(12):2161–2165. [PubMed: 12461333]
34. Nakamizo M, Yokoshima K, Yagi T. Use of free flaps for reconstruction in head and neck surgery: A retrospective study of 182 cases. Auris Nasus Larynx. 2004; 31:269–273. [PubMed: 15364362]
35. Ross DA, Hundal JS, Son YH, et al. Microsurgical free flap reconstruction outcomes in head and neck cancer patients after surgical extirpation and intraoperative brachytherapy. Laryngoscope. 2004; 114:1170–1176. [PubMed: 15235342]
36. Shaari CM, Buchbinder D, Costantino PD, Lawson W, Biller HF, Urken ML. Complications of microvascular head and neck surgery in the elderly. Arch Otolaryngol Head Neck Surg. 1998; 124(4):407–411. [PubMed: 9559687]
37. Imaizumi N, Monnier Y, Hegi M, Mirimanoff RO, Rüegg C. Radiotherapy suppresses angiogenesis in mice through TGF-βRI/ALK5-dependent inhibition of endothelial cell sprouting. PloS one. 2010; 5(6):e11084. [PubMed: 20552031]

38. Donneys A, Deshpande SS, Levi B, Buchman SR. Real-time investigation of the angiogenic effect of deferoxamine on endothelial cells exposed to radiotherapy. Plastic and Reconstructive Surgery. 2013; 131(5S):141.

39. Andreassen CN, Grau C, Lindegaard JC. Chemical radioprotection: A critical review of amifostine as a cytoprotector in radiotherapy. Semin Radiat Oncol. 2003; 13:62–72. [PubMed: 12520465]

40. Wasserman TH, Brizel DM, Henke M, et al. Influence of intravenous Amifostine on xerostomia, tumor control, and survival after radiotherapy for head-and-neck cancer: 2-year follow-up of a prospective, randomized, phase III trial. Int J Radiat Oncol Biol Phys. 2005; 63(4):985–90. [PubMed: 16253773]

41. Kouvaris JR, Kouloulias VE, Vlahos LJ. Amifostine: the first selective-target and broad-spectrum radioprotector. The oncologist. 2007; 12(6):738–747. [PubMed: 17602063]

42. Capizzi RL, Scheffler BJ, Schein PS. Amifostine-mediated protection of normal bone marrow from cytotoxic chemotherapy. Cancer. 1993; 72(S11):3495–3501. [PubMed: 8242582]

43. Forrest CR, O'Donovan DA, Yeung I, et al. Efficacy of radioprotection in the prevention of radiation-induced craniofacial bone growth inhibition. Plastic and reconstructive surgery. 2002; 109(4):1311–23. [PubMed: 11964983]

44. Damron TA, Spadaro JA, Margulies B, et al. Dose response of amifostine in protection of growth plate function from irradiation effects. Int J Cancer. 2000; 90:73–9. [PubMed: 10814957]

45. Damron TA, Margulies B, Biskup D, et al. Amifostine before fractionated irradiation protects bone growth in rats better than fractionation alone. Int J Radiat Oncol Biol Phys. 2001; 50:479–83. [PubMed: 11380237]

46. Brittenham GM. Iron-chelating therapy for transfusional iron overload. N Engl J Med. 2011; 364:146–156. [PubMed: 21226580]

47. Semenza GL. Hydroxylation of HIF-1: oxygen sensing at the molecular level. Physiology. 2004; 19(4):176–182. [PubMed: 15304631]

48. Wang GL, Semenza GL. Desferrioxamine induces erythropoietin gene expression and hypoxia-inducible factor 1 DNA-binding activity: implications for models of hypoxia signal transduction. Blood. 1993; 82(12):3610–3615. [PubMed: 8260699]

49. Blatt J, Taylor SR, Stitely S. Mechanism of antineuroblastoma activity of deferoxamine in vitro. J Lab Clin Med. 1988; 112:433. [PubMed: 2459279]

50. Hann HWL, Stahlhut MW, Hann CL. Effect of iron and desferoxamine on cell growth and in vitro ferritin synthesis in human hepatoma cell lines. Hepatology. 1990; 11:566–569. [PubMed: 2158479]

51. Hann HWL, Stahlhut MW, Rubin R, Maddrey WC. Antitumor effect of deferoxamine in human hepatocellular carcinoma growing in athymic nude mice. Cancer. 1992; 70:2051. [PubMed: 1327484]

52. Donfrancesco A, Deb G, Dominici C, Pileggi D, Castello MA, Helson L. Effects of a single course of deferoxamine in neuroblastoma patients. Cancer Res. 1990; 50:4929–4930. [PubMed: 2379156]

Highlights

- We examine a combination treatment for radiation-induced changes to bone healing
- Angiographic modeling, histology and biomechanics quantified bone healing
- Investigation of combined amifostine plus deferoxamine treatment is reported

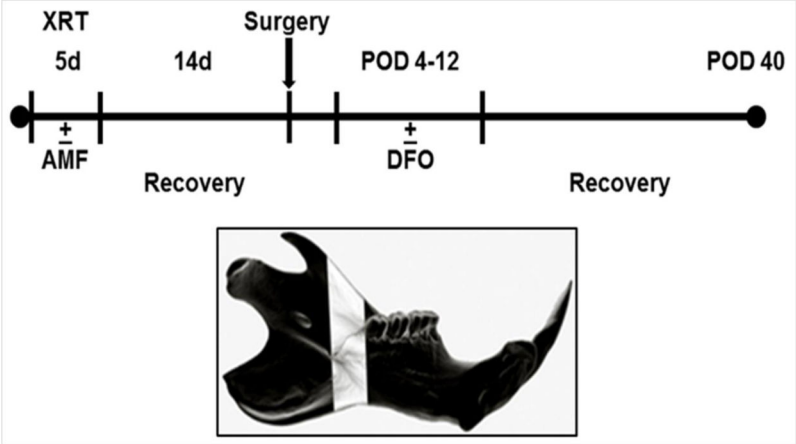

Figure 1.
(Top): Experimental timeline. (Bottom): Schematic left hemi-mandible demonstrating the region of interest (ROI) highlighted in white.

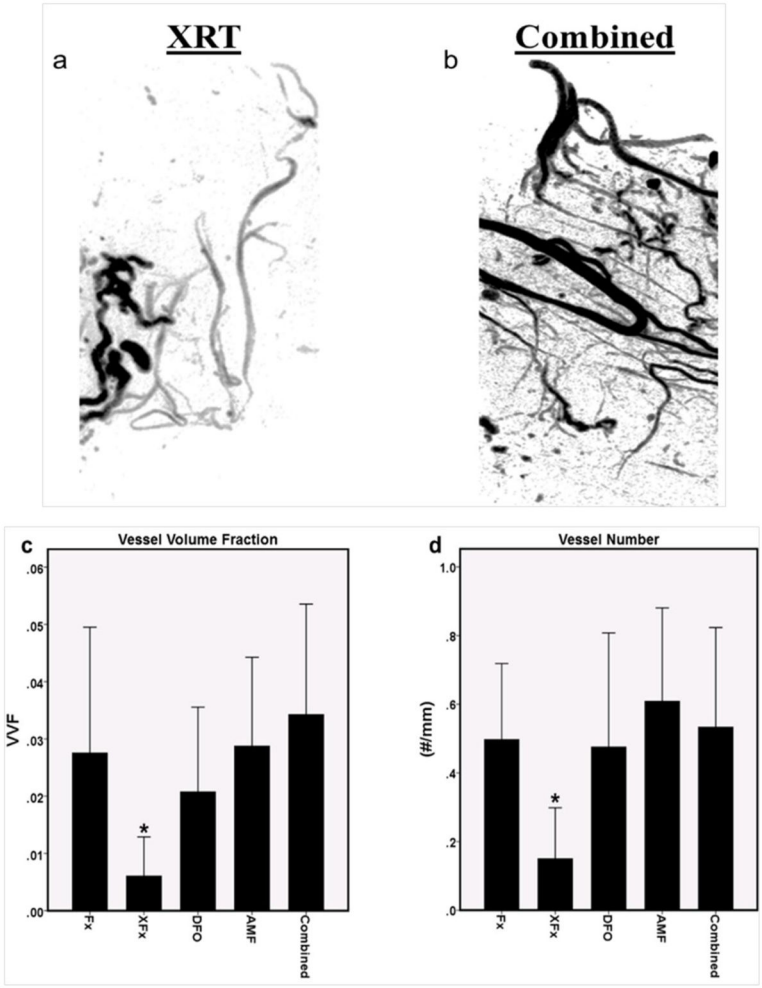

Figure 2.

Analysis of vascularity: (a and b) Representative angiogram reconstructions of the region of interest depicting the XRT and Combined groups. Note the diminution of blood vessel volume and altered morphology after radiation treatment that is not present with combined therapy. (c and d) 3D angiographic modeling metrics for Vessel Volume Fraction (VVF) and Vessel Number, respectively. *: $p < 0.05$.

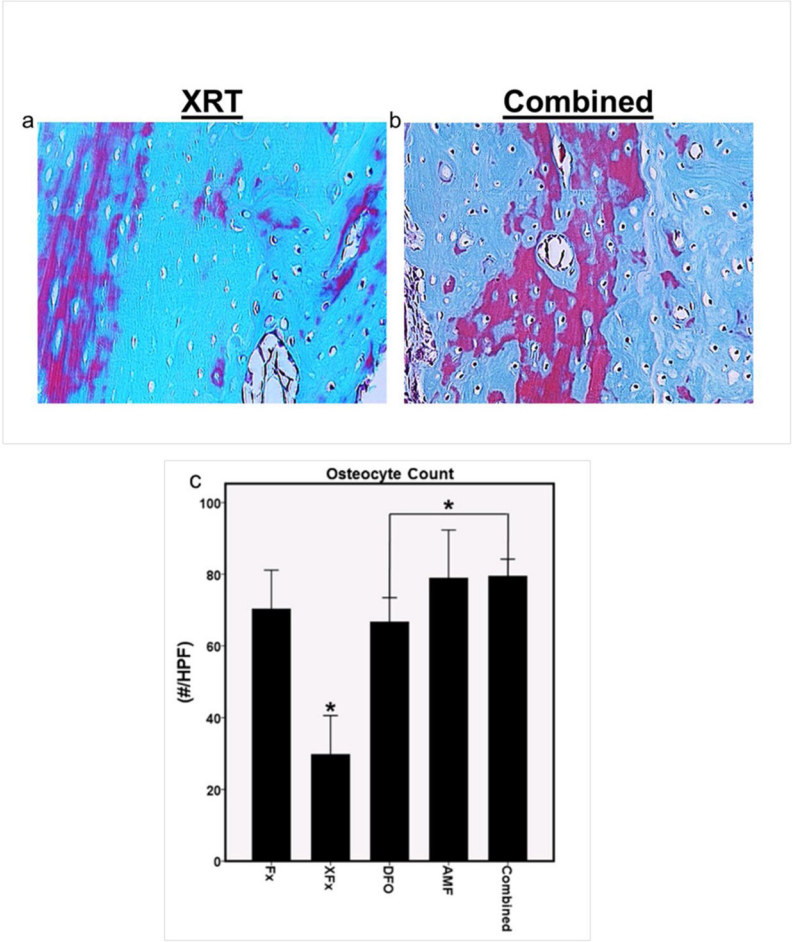

Figure 3.

Histological analysis: (a and b) Representative 16x high power field sections with Gomori's trichrome stain, demonstrating the diminution of osteocytes in lacunae within irradiated bone, and the comparative sparing of osteocytes observed with combined therapy. (c) ROI osteocyte count metric. *: $p < 0.05$

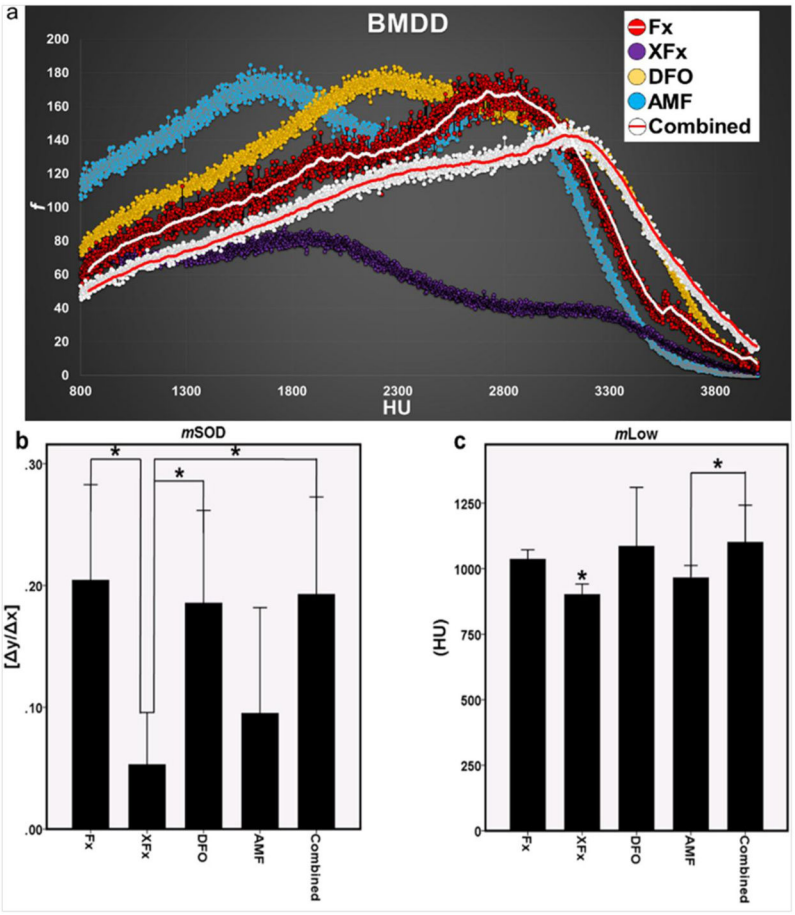

Figure 4.

BMDD analysis: (a) Graphic depiction of group histograms visually highlighting the similarity of the Combined curve to that of Fx. (b and c) BMDD metrics of mineralization slope of decline and mineralization-low. *: $p < 0.05$

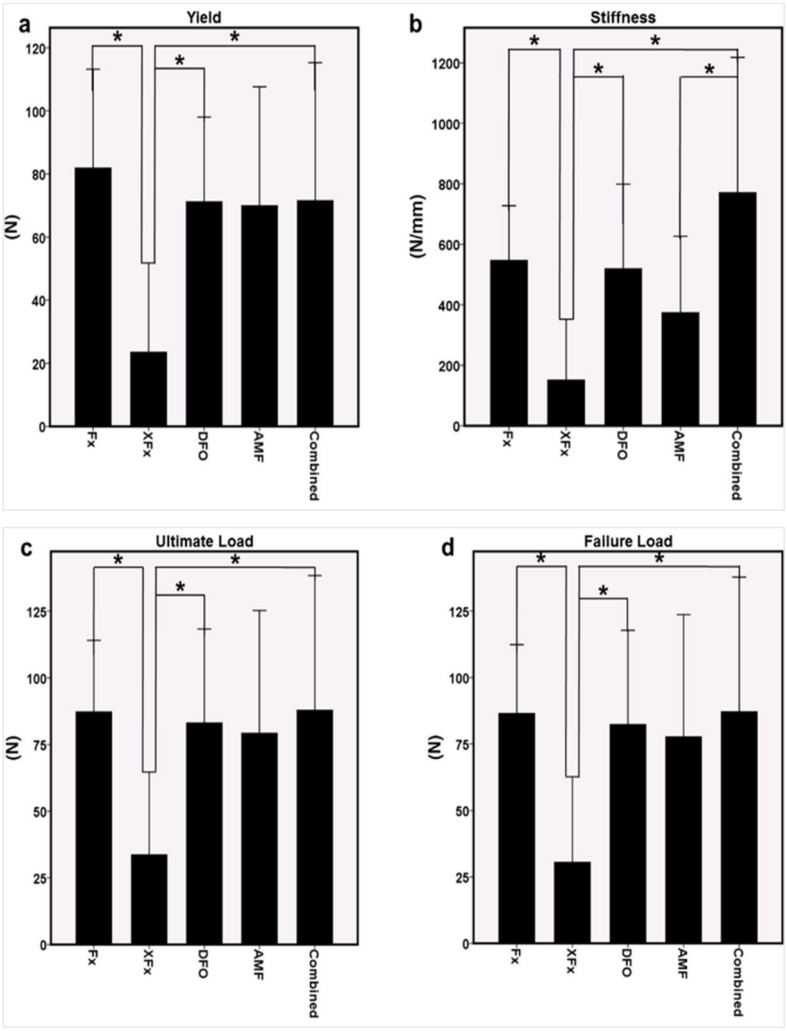

Figure 5.
(a–d) Mechanical metrics of yield, stiffness, ultimate load and failure load. *: $p < 0.05$